THE EFFECT OF SHROUD DESIGN ON FLOW STRUCTURE AT THE TIP AREA AND STAGE EFFICIENCY

A.Granovskiy *I.Afanasiev* *E. Marchukov*
andrey.granoskiy@yandex.ru
Lyulka Design Bureau
Moscow, Russia

ABSTRACT

Last blades of heavy-duty gas and steam turbines have shrouds to avoid dangerous resonance frequency. In this paper, a numerical investigation of the flow structure around full and partial shrouds with various geometries and the effect of the various shrouds on the turbine stage efficiency are carried out. Moreover, stage efficiencies for shrouded and unshrouded blades are compared. Taking into account the fact that shrouds run in high temperature conditions, the adiabatic temperature distribution on the shroud surface is analyzed. In particular, effect of the vortex system downstream of the shroud fin and features of the shroud geometry on the non-uniform heating of the shroud surface is demonstrated. Two methods have been used to cool the shroud: cool air injection into a cavity upstream of the shroud and through profiled slot downstream of the fin. In order to validate numerical results, experimental data of a turbine stage with shrouded blade was used.

KEYWORDS: PARTIAL AND FULL SHROUD, FLOW STRUCTURE, LOSSES AND STAGE EFFICIENCY

NOMENCLATURE

P^*_0 inlet total pressure
T^*_0 inlet total temperature
G mass flow
N outlet power
P^*_{1w} total pressure in relative motion
T^*_{1w} total pressure in relative motion
β_1 inlet flow angle
P_2 outlet static pressure
P^*_2 outlet total pressure
h blade span
δ tip clearance
δ/h relative tip clearance
k specific heat ratio, $k= c_p/c_v$
c_p specific heat capacity at constant pressure
c_v specific heat capacity at constant volume
R gas constant; radius
R/h relative height of flowpath
n rotation speed, rpm
ζ losses
ρ reaction
η total- to- total efficiency;
$\delta\eta$ stage efficiency change

Subscripts:
0 stage inlet
1 rotor inlet
2 stage or rotor exit

Acronyms:
PS pressure surface
SS suction surface
LE leading edge
TE trailing edge

INTRODUCTION

In the last two decades a lot of papers regarding the effect of the shroud design on the flow structure, tip clearance losses and turbine efficiency have been issued. While basic aspects of the issue at hand were studied by Denton (1993), further development of numerical methods allowed detailed investigation of features of the vortex structure in the tip area. Harley (2004) and Wallis et al. (2000) outlined the shroud leakage phenomena impacting on the turbine performance. Those are: mixing in the shroud inlet cavity, mixing through the labyrinth seal, mixing in the exit cavity due to velocity differential between the cavity reentry flow and the main flow. Afterwards, this scheme has been investigated by many researches, including Pfau et al. (2004), Porreca et al. (2005). In an experimental study of three plane cascades: one with full shroud and two with partial shrouds, carried out by Nirmalan and Bailey (2005), the full shroud demonstrated the lowest performance loss compared to both partial tip shrouds. The full tip shroud geometry at larger clearance gap had the same performance as the medium and deep scallop at the lower clearance gaps. Gier et al. (2006) performed a loss breakdown for inner and outer cavities and concluded that 60% of the losses are due to the mixing during leakage flow re-entry. Therefore, controlling the path of the exiting leakage flow is crucially important. Strong counter-rotating vortices dominating secondary flows at the interaction zone have also been reported by Adami et al. (2006). Porreca et al. (2007) studied three variants of shroud design: full shroud, partial shroud and enhanced partial shroud. The investigation showed that the use of partial shroud decreases aerodynamic efficiency by 1% in comparison with the full shroud case and optimized partial shroud decreases aerodynamic efficiency by 0.5%. Rosic et al. (2007) found that reducing length of both the inlet and the exit shroud cavities is beneficial, so the cavities should be reduced as much as the turbine's operational conditions allow. Barmpalias et al. (2012) investigated the effect of rotor inlet cavity volume on efficiency. As a result, efficiency increased by 1.1% and 1.6% for the 14% and 28% cavity volume reduction respectively. Notable results have been obtained by Yoon et al. (2014) in comparison of stages with shrouded and unshrouded blades. Tests showed that there was a certain "break-even clearance" at which both shrouded and unshrouded stages had the same efficiency. At tip clearances less than the break-even clearance efficiency of the unshrouded stage was higher than that of the shrouded, and the difference between shrouded and unshrouded stages at zero clearance was termed the "offset loss". Guyader et al. (2016) studied a two-stage low-pressure turbine (LPT) with axisymmetric and asymmetric tip shrouds to better understand the complex flow created by them in order to develop simple models to guide aeromechanical designs. They found that the stage efficiency decreased when scalloped tip shroud geometries were used. Moreover, they found that this penalty seemed to be caused by the cavity exit much more than the inlet. Granovskiy and Afanasiev (2017) investigated seven types of partial shroud geometry in order to choose the best variant. They also showed how to control vorticity around the shroud by adjusting the volume of the cavities.

In this paper, the numerical investigation of the flow structure around full and partial shrouds with various geometries was conducted and the effect of various shroud geometries on the flow structure around shroud, losses and turbine stage efficiency analysed. Moreover, two variants of the cooling air injection to cool the shroud platform were investigated. Validation of the numerical results was done by comparison between numerical and test data for an experimental turbine stage with shrouded blade.

Features of investigated variants

The space around the tip part of the rotor blade remains one of the most important sources of losses in turbomachines. In particular, in cooled turbines complicated flow pattern at the tip area of rotor blades is the main cause for the loss generation. The design features of both the open tip clearance (unshrouded) and shrouded blades mentioned in Introduction show how difficult it is to

take into account all of these features to describe the flow within the tip clearance. State-of-the-art numerical methods present an opportunity to visualize the flow structure at the tip area and estimate quantitatively the losses caused by its features. The table shows the variants examined.

Table : Variants of the tip area design

Variants	Type of shroud	δ mm	δ/h %	View of variants
1	Partial with one fin	0	0	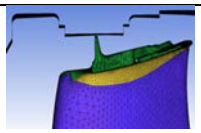
2	Partial with one fin	0.4	0.3	
3	Partial with one fin	1.4	1.1	
4	Full with one fin	0.0	0.0	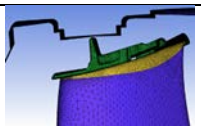
5	Full with one fin	0.4	0.3	
6	Full with one fin	1.4	1.1	
7	Without shroud	0.4	0.3	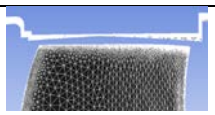
8	Without shroud	1.4	1.1	
9	Air injection into inlet cavity; partial shroud	1.4	1.1	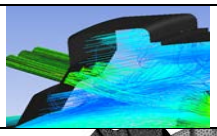
10	Air injection through profiled slot on full shroud	1.4	1.1	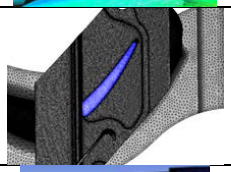
11	Full shroud with front fin	0,4	0,3	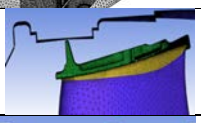
12	Partial shroud with two fins	0,4	0,3	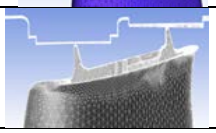

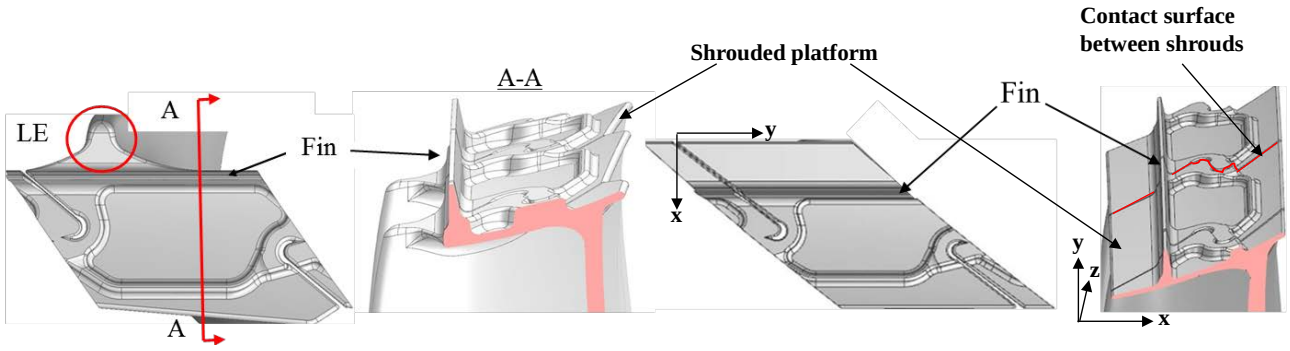

a) b)

Figure 1: Shape of the shroud (Variants 1-6); a) partial shroud; b) full shroud

Figure 1 shows view of partial shroud and full shroud with one fin which were investigated in this study (Variants 1 – 6). In Figure 1a it is seen that the partial shroud does not cover LE of the blade.

At the same time the full shroud covers the entire tip section of the blade. Axonometric views of shrouded platforms (shrouds) in Figure 1 show contact surfaces between shrouds. All of the platforms together form the entire shrouded ring. Variants 7 and 8 are unshrouded with values of tip clearance $\delta/h = 0.3\%$ and 1.1% correspondingly. In Var.9 cooling air is fed through three holes within the scope of the numerical domain for one blade into the inlet cavity upstream of the shroud. In Variant 10 cooling air is fed through a profiled slot in the shroud downstream of the fin.

Numerical approach

The numerical investigation of blades with the various shroud geometries from Table was carried out by means of the commercial program complex ANSYS FLUENT. Figure 2a shows the numerical domain which is a sector of the cylinder containing the blade with the shroud, hub platform and casing at the tip area corresponding to the real design cavities and honeycomb fillings over the shroud as well as view of the unstructured numerical grid on the blade surface. The mesh was produced by the proprietary grid generator ANSYS ICEM 17.0. Figure 2a presents the numerical domain and on the LE, TE and shroud regions the number of cells is increased in order to refine the shroud geometry. The total cell count spans from 13.4×10^6 up to 16×10^6 depending on the shroud shape and the tip clearance value and for unshrouded variants it is about 5×10^6. The quality of the numerical mesh near the walls is confirmed by the view of the mesh and the y^+ distribution along the blade surface presented in Fig.2b. The value of y^+ is ≤ 0.3 near the walls due to cell size decreasing exponentially in the wall area; this confirms the high quality of the numerical grid used.

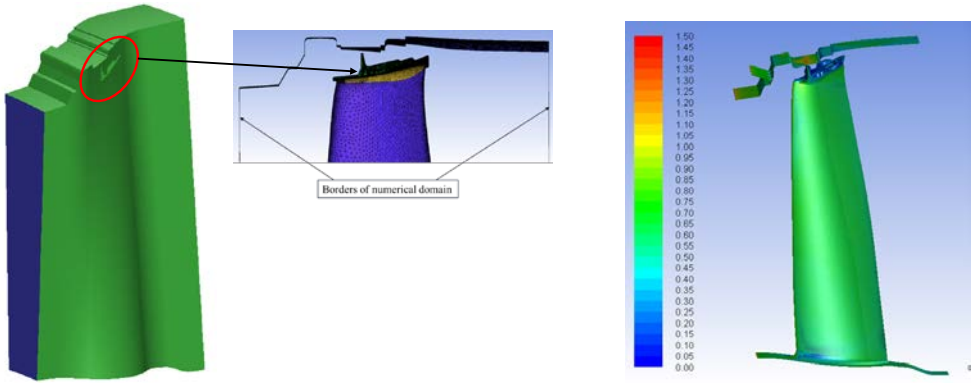

a) b)

Figure 2: View on the numerical domain and tip part of the flow path
a - numerical domain and view on the tip part of the blade with unstructured numerical grid
b - distribution of the y^+ function along the blade surface for Var. 9

All calculations were carried out using the Realizable k-ε turbulence model and a numerical scheme of second order accuracy with the inlet turbulence intensity Tu = 10%. Cylindrical coordinates in a frame of reference rotating about the turbine axis with angular velocity ω = 1256.64 rad/s were used. In this case convergence of the solution is obtained at 1000 – 3000 iterations depending on the size of the numerical grid and computational strategy. The tip clearances considered were δ = 0; 0.4 mm; 1.4 mm which corresponds to the relative tip clearances δ/h = 0; 0.3%; 1.1% respectively.

The same boundary conditions were applied to calculations for every investigated variant. The boundary conditions correspond to one of the working modes of the unit. Figure 3 shows view of the total pressure distributions P_{1w}^*, total temperature distribution T_{1w}^* and inlet flow angle β_1 in the rotating frame as specified at the inlet boundary of the numerical domain; the static pressure

distribution P_2 is specified at the exit. Exit Mach number in relative motion at the tip area was M_{2w} = 0.82 and exit Mach number in absolute motion at the mid of span was M_2=0.44.

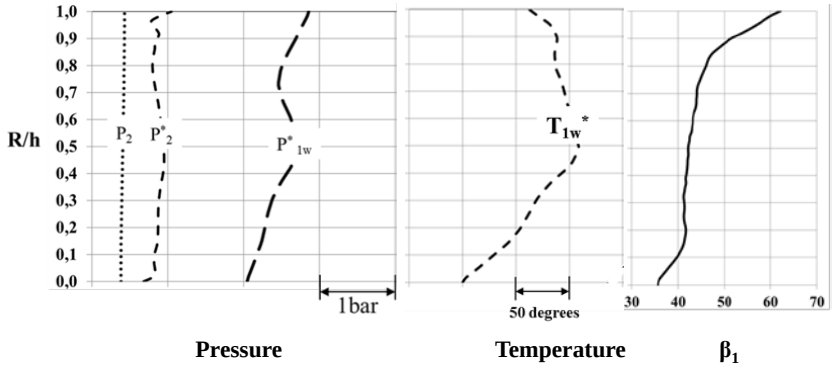

Figure 3: Boundary conditions for calculations of all variants by FLUENT

Experimental approach

The experimental results were obtained from a LP turbine stage in order to validate the CFD simulations used in this study. The scheme of the test rig with the tested turbine stage and table with the test data parameters at the design point are shown in Fig. 4.

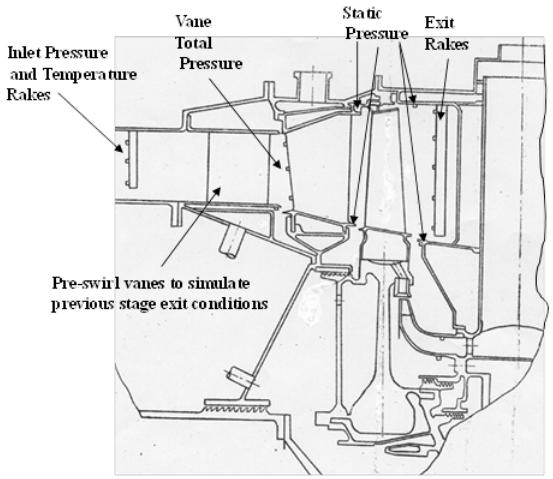

Parameter	Unit	Value
Inlet total temperature	K	720
Inlet total pressure	bar	2.5
Reduced flow capacity	$sm^2K^{0.5}/sec$	420.0
Outlet total pressure	bar	1.19
Total pressure ratio		2.1
Stage inlet flow angle	degree	62
Relative tip clearance	%	0.85
Reduced rotation speed	$rpm/K^{0.5}$	285

Figure 4: Scheme of the test rig with the experimental LPT stage

The test LPT was simulated by the FLUENT code. The boundary conditions corresponded to the test conditions; the entire stage was simulated for validation purposes. Figure 5 shows the comparison between test efficiency and computed stage efficiency against reduced rotor rotation speed $n/\sqrt{T_0^*}$ over the range of 270 to 305. Calculations were conducted for $n/\sqrt{T_0^*}$ =270; 285; 300. It is seen that the computed stage efficiency is a little higher than the efficiency measured in the experiment. In general the difference between experimental and numerical efficiency is less than 0.5%.

Figure 6a shows the comparison between the experimental and numerical results for exit Mach number M_2 and flow angle α_2 against reduced rotor rotation speed $n/\sqrt{T_0^*}$ over the range 270 to 305. The correlation between test and numerical data is quite satisfactory. The static pressure was measured in the axial gap at six static tappings both on the inner and outer surfaces of the flow path. In Figure 6b it is seen that the measured reaction corresponds well to the computed values.

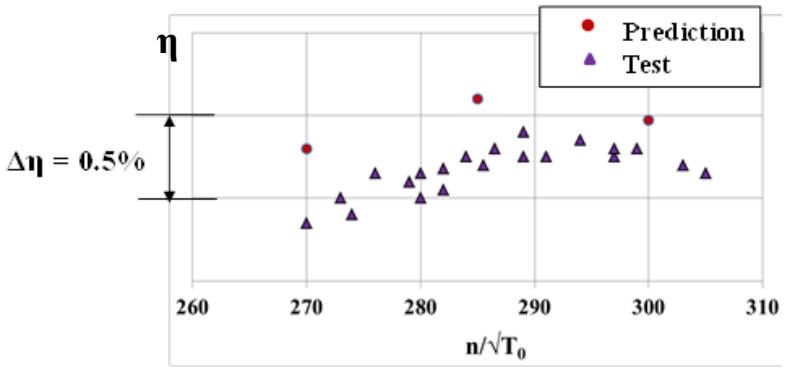

Figure 5: Comparison between test and numerical data for LPT stage efficiency

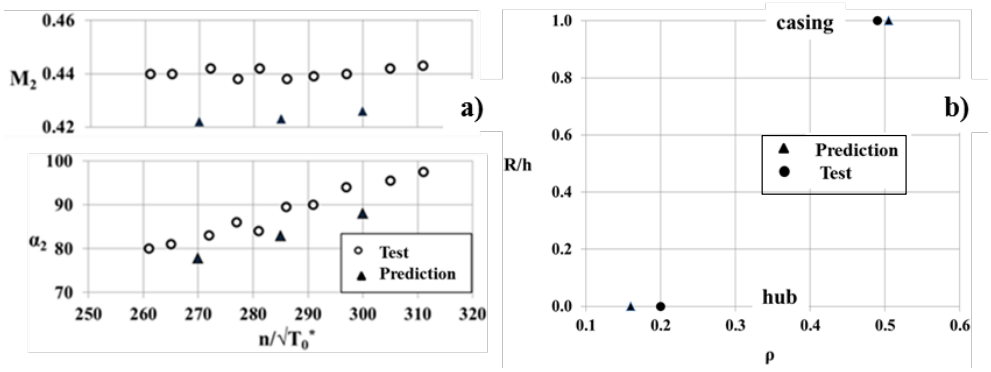

Figure 6: Comparison between test and numerical data
a - exit Mach number M2 and flow angle α_2; b - reaction

Thus the validation of the numerical approach by comparison between the experimental and numerical data for the experimental LPT stage confirmed reliability and credibility of numerical approach used in this research.

Flow structure around the shroud

Figure 7 shows the flow structure around the partial shroud for variants 2 and 3. There is a large vortex in the inlet cavity upstream of the fin. It is seen that due to uncovered LE an intensive leaking flow from pressure side to suction side appears. This part of the main flow feeds the secondary flows and increases secondary losses.

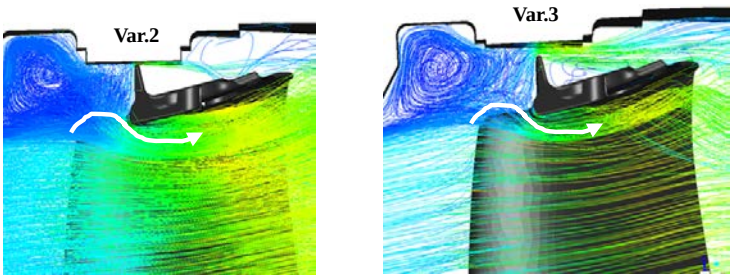

Figure 7: Flow structure around partial shroud (lines M = const); Variants 2, 3

In order to better demonstrate variation of the vortex structure along the shroud in circumferential direction, the streamline distributions in 6 different longitudinal sections (y_i=const) of the numerical domain (Figure 8a) have been composed into pseudo-3D figures 8b and 8c. It is seen that the

vortex in the inlet cavity changes its intensity along the shroud in both variants due to the change of the partial shroud geometry in front of the fin. The vortex system downstream of the fin consists of two intensive ellipsoidal counter-rotating vortices. This vortex system has almost constant structure along the shroud for Var.2 for relative tip clearance δ/h = 0.3%. The increase in tip clearance to δ/h = 1.1% for Var. 3 resulted in a significant change of the vortex system downstream of the fin. Some vortices disappeared and other became less intensive. Consequently, sealing properties of these vortices diminished.

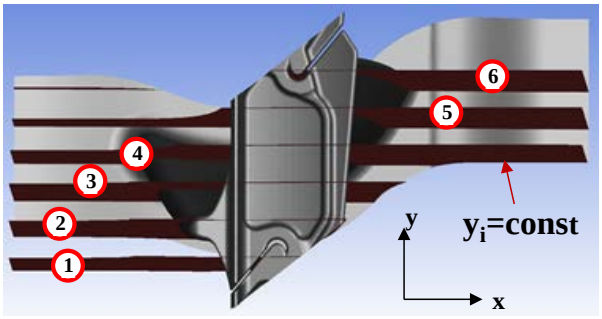

a)

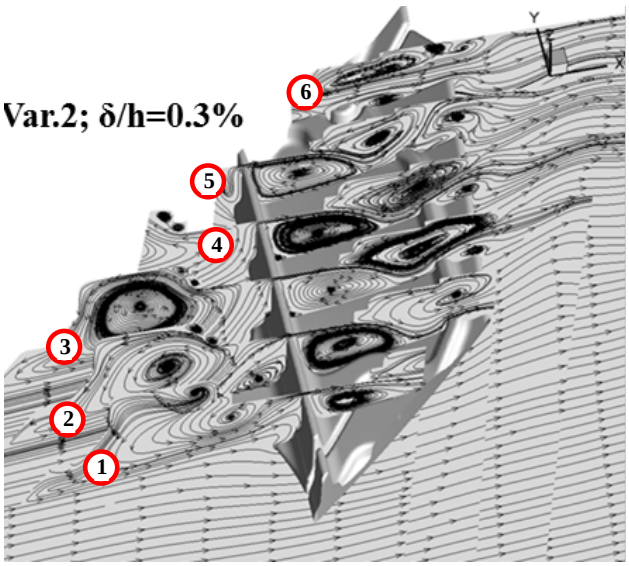

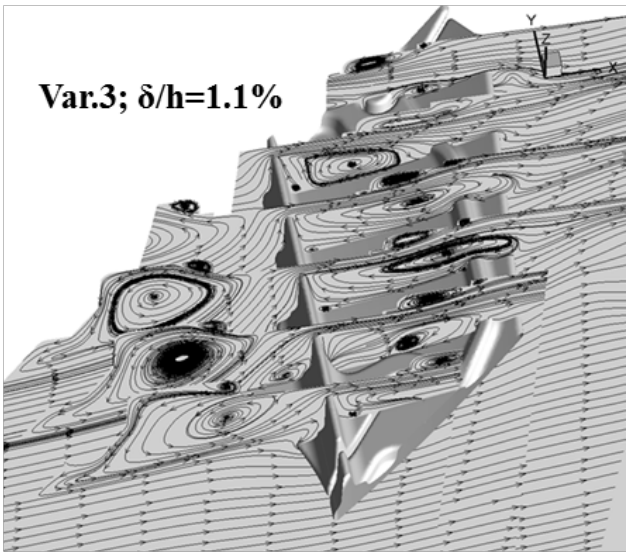

b) c)

Figure 8: The flow pattern around partial shroud Var.2 and Var.3; a – view from above on the partial shroud with sections 1-6; b – vortex structure around the shroud in Var.2; c – vortex structure around the shroud in Var.3

The use of the full shroud resulted in decrease of the flow from pressure side to suction side upstream of the LE. In Figure 9 it is seen that due to the fully covered LE the vortex structure upstream of the fin has changed in comparison with the inlet vortex structure for the partial shroud. In the full shroud case the form and intensity of the inlet vortex became more uniform. Moreover, an additional vortex in front of the fin appeared. As a result, the sealing produced by the vortex system of the full shroud is more effective as compared with the partial shroud.

The complicated vortex system around the partial shroud with two fins of Var.10 in sections A-A, B-B and C-C is shown in Figure 10b. It is seen that the number of vortices and their shape change from one section to another in the circumferential direction. In section A-A the bottom of

the inlet vortex is close to the fin. Then the shape of this vortex changes through the sections B-B and C-C. The red line in the section B-B shows the tip clearance leakage path. Downstream of the first fin the leakage flow passes between the two vortices located between the fins. The second vortex pushes the leakage flow onto the shroud surface and then the flow goes through, over the second fin, into the area downstream of the shroud. The inlet vortex and the vortices between the fins play a positive role to block and/or reduce the tip clearance leakage.

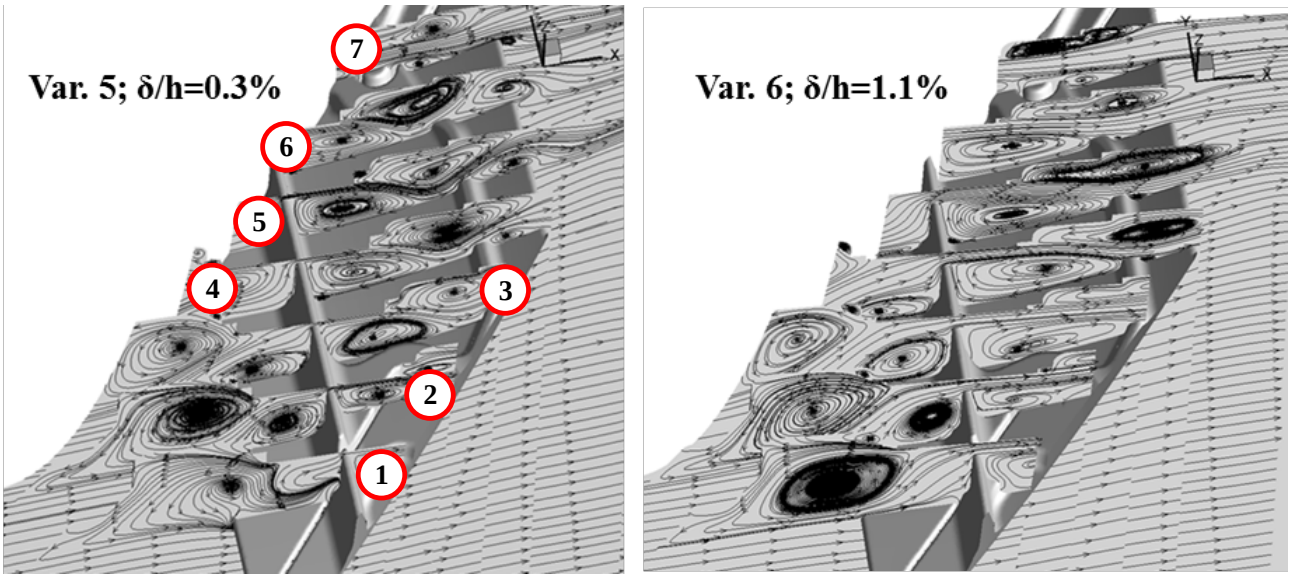

a) b)

Fig.9. The flow pattern around full shroud Var.5 and Var.6; a – vortex structure around shroud in Var.5; b – vortex structure around shroud in Var.6

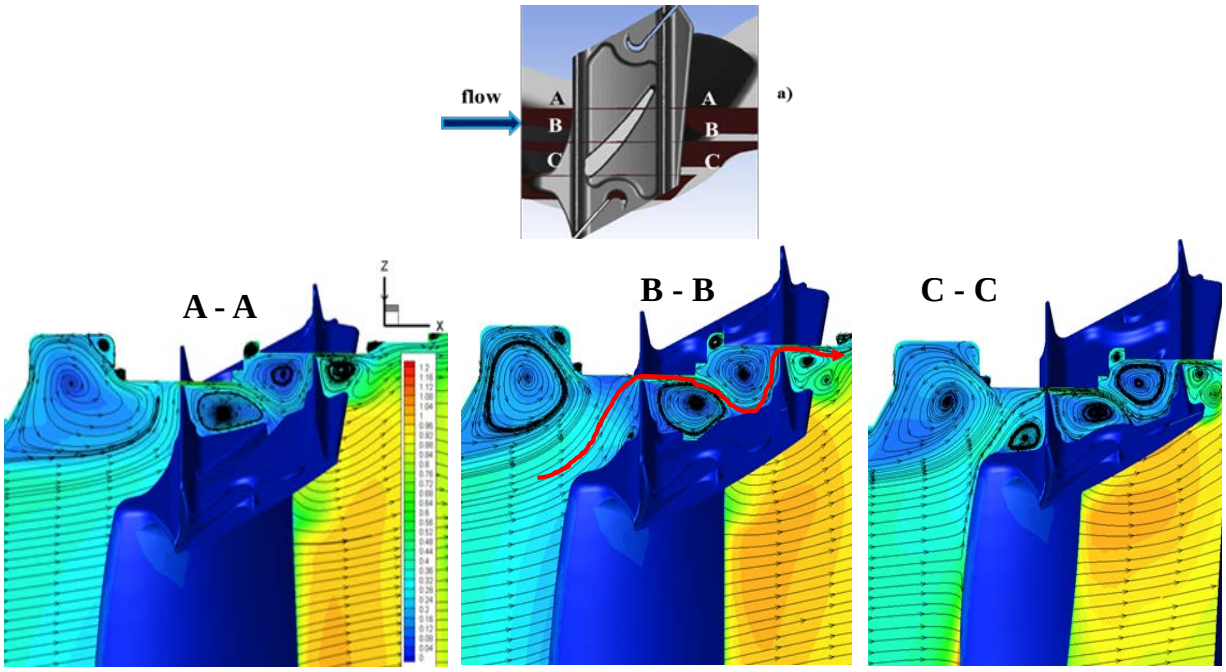

b)

Figure 10: Flow structure around partial shroud with two fins; Variant 12 a - view from above on partial shroud with two fins and sections A-A, B-B, C-C; b – distribution of lines Mach = const in the noted sections

Losses and stage efficiency

A comparison of the computed loss for the partial and full shroud at relative tip clearances δ/h = 0; 0.3% and 1.1% is presented in Figure 11. Radial loss distributions in Figure 11a show that the difference is localized to just within the shroud space. The rest of the blade span (R/h = 0 - 0.8) has nearly the same losses. Figure 11b shows the difference between total losses for the partial shroud and for the full shroud over the range of relative tip clearances from 0 to 1.1%.

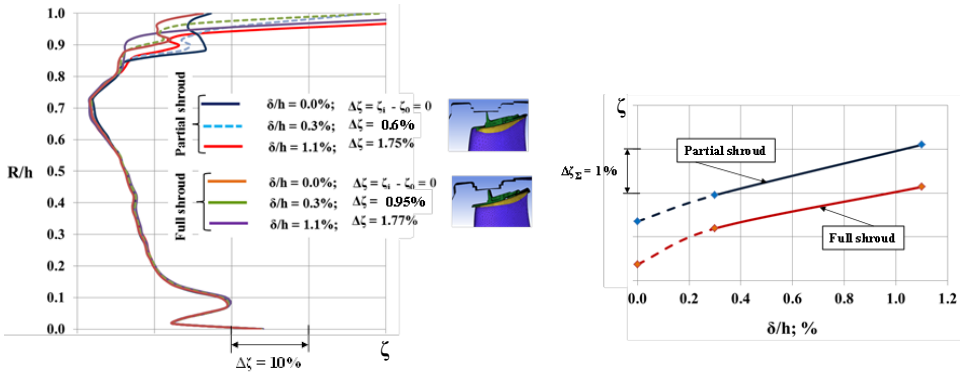

a) b)

Fig 11: Losses for blades with partial and full shroud
a – loss radial distribution; b – loss vs relative tip clearance

The quantitative effect of various shroud geometries is compared as respective stage efficiencies calculated by means of expression (1) for total- to-total efficiency:

$$\eta = \frac{N/G}{\frac{k}{k-1} R \cdot T_0^* \cdot \left(1 - \left(p_2^*/p_0^*\right)^{\frac{k-1}{k}}\right)} \qquad (1)$$

The dependence between the stage efficiency η and the relative tip clearance δ/h for stages with shrouded and unshrouded is presented in Figure 12. It is necessary to point out that the computed stage efficiency at zero clearance is only nominal, because in this case the vortex system is generated solely by the secondary flows and not as a result of interaction between the tip clearance leakage and the main flow. This plot shows that at δ/h < 1.35% the stage with the unshrouded blade has better efficiency than the stage with the partially shrouded blade, with "offset loss" as defined by Yoon et.al (2014) δη ≈ 1% near δ/h = 0. As for the stage with the fully shrouded blade, it becomes less efficient at δ/h < 0.53% with "offset loss" around δη ≈ 0.5% near δ/h = 0. These results can be used as a justification for use of unshrouded blades on the condition that the minuscule tip clearance is secured by a special control system.

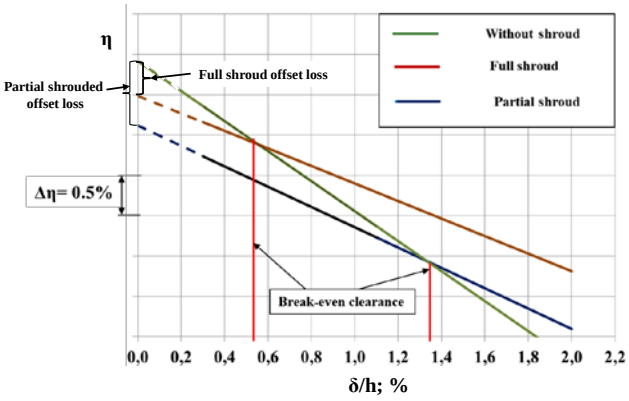

Figure 12: Stage efficiency vs relative tip clearance for shrouded and unshrouded blade

Figure 13 shows the comparison of stage efficiency for some variants of shrouded blades against the unshrouded blade at the relative tip clearance values δ/h = 0.3% and 1.1%. It is seen that for δ/h = 0.3% the unshrouded blade has an advantage over the shrouded blade variants. However, for δ/h = 1.1% the blade with the full shroud is the most efficient.

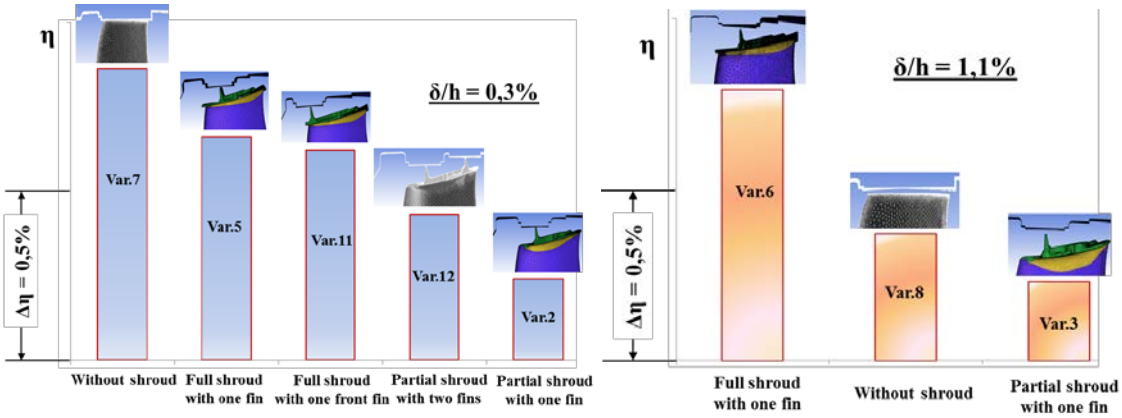

Fig. 13: Stage efficiency for various designs of blade tip area at δ/h = 0.3% and δ/h = 1.1%

Temperature distribution in the tip area

Figure 14 shows the distribution of isotherms of the total relative temperature T_w^* over the shroud and the adiabatic temperature distribution T_{wall} on the outer surface of the partial shroud Var.3 and the full shroud Var.6. Due to the location of the upstream vortex the non-uniform isotherm distribution in circumferential direction is observed for both variants. This results in hot streaks over the shroud. The high temperature spots can be seen on the outlet part of the shrouds.

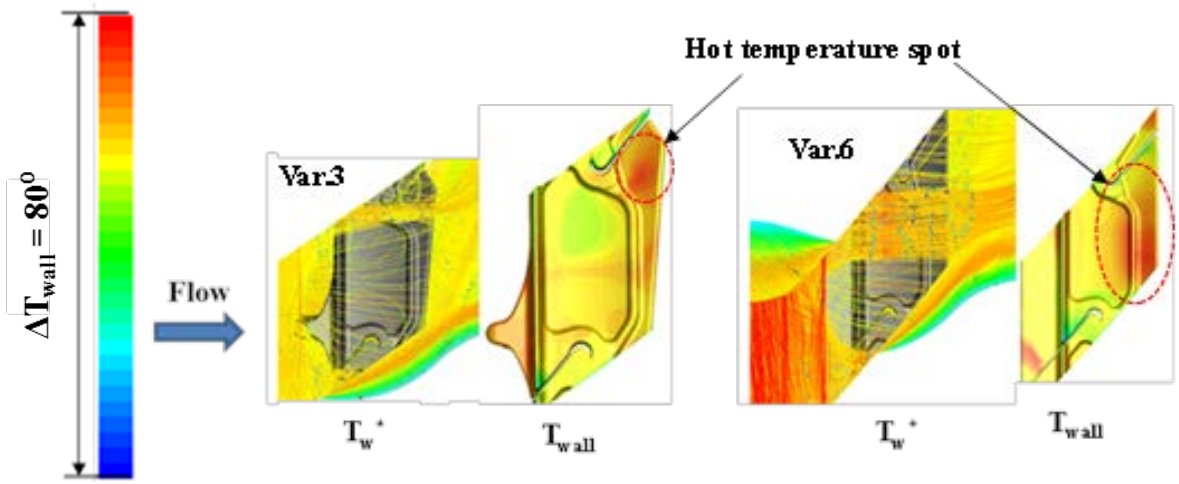

Figure 14: Total flow temperature T_w^* and adiabatic temperature T_{wall} distributions

Figure 15 shows distributions of the wall adiabatic temperature on the inner surface of the shroud for Var.3 and Var.6. Figure 15a shows that due to the leakage from the pressure surface to the suction surface near the LE and the enhancement of the secondary flows, shroud overheating near the pressure side occurs for the partial shroud Var.3. On the inner surface of the full shroud in Figure 15b the level of the wall temperature near the airfoil is less than for Var.3.

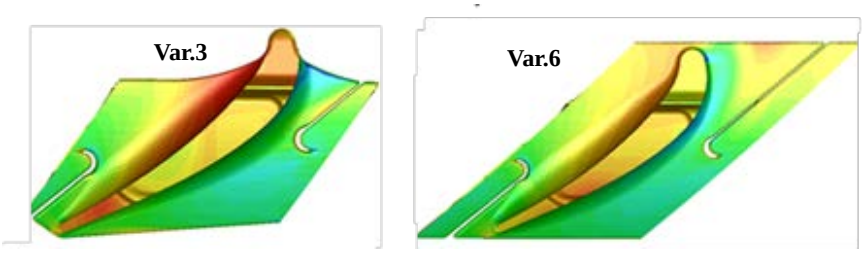

a) b)

Figure 15: Adiabatic temperature T_{wall} on the inner surface of the shroud
a – partial shroud Var.3; b – full shroud Var.6

In order to minimize the risk of overheating two approaches were used:

- cool air injection into the inlet cavity (Var. 10, Figure 2b)
- cool air injection through a profiled slot on the full shroud (Var. 10, from Table 1).

Cool air injection into the inlet cavity

In order to decrease the temperature over the shroud, cool air is injected into the inlet cavity through three pipes within one pitch of the blade as shown in Figure 2b. The idea is, on one hand, to mix the cool air with the part of the main stream within the inlet cavity to decrease flow temperature in front of the shroud and, on the other hand, to change the vortex structure as a result of cool air interacting with the vortices. The relative cool air mass flow is G_{cool}/G_{gas} = 0.6%. Figures 16a and 16b show the adiabatic wall temperature distribution T_{wall} on the shroud for Var.3 and Var.9. It is seen that the cooling air injection through pipes into the inlet cavity has changed the vortex structure in front of the fin. Due to this fact the hot spot on the shroud surface for Var.9 became larger than in Var.3. Moreover, it moved from the left part of the shroud in Var.3 to the central part of the shroud in Var.9. Figure 16c shows the total flow temperature T_w^* distribution in relative motion around the shroud for Var.9. It is seen that the mixed flow from the inlet cavity passes through the tip clearance and onto the outlet part of the shroud. As a result, the tip clearance leakage has increased by $\delta G_{\text{radial gap}}$ = 0.6% due to the increase in the mixed flow density in comparison with Var.3. In this case the stage efficiency drop is $\delta\eta$ =0.34% as compared with Var.3.

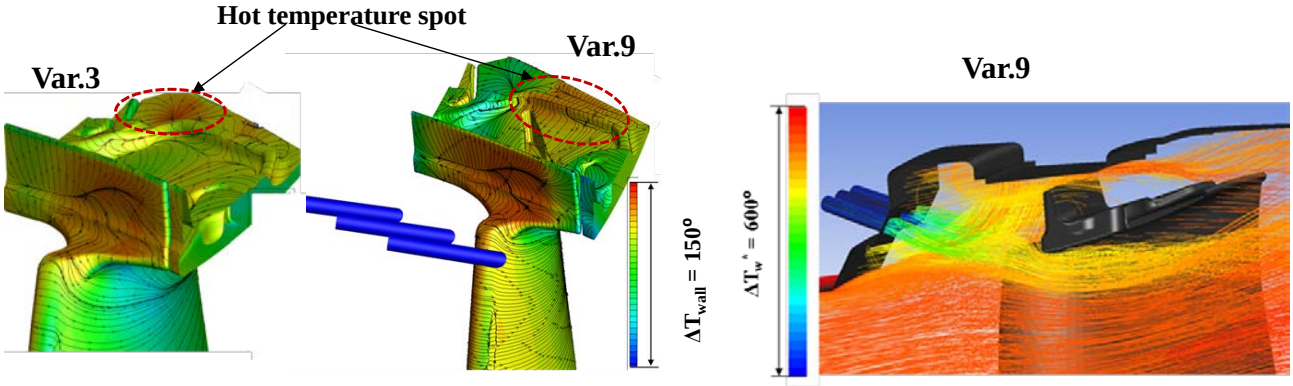

a) b) c)

Figure 16: Temperature distribution at the tip area for Var.9
a - adiabatic wall temperature distribution T_{wall} on the shroud for Var.3
b - adiabatic wall temperature distribution T_{wall} on the shroud for Var.9
c - total flow temperature T_w^* distribution in relative motion for Var.9

Cooling air injection through profiled slot on full shroud

Another option for shroud cooling is to inject cool air through a profiled slot on the shroud. In this case cool air isolates the outer shroud surface from the hot gas passing through the tip clearance. Figure of Var.10 from Table 1 shows a top view on the shroud with numerical grid on the shroud surface including the profiled slot for cool air injection. The fine mesh near the wall allows taking all of the features of shroud geometry into account. Numerical grid contained 14.6×10^6 cells. The streamline distributions and total temperature distributions T_w^* in the seven sections for Var.6 and Var.10 are presented in Figures 17. In Figure 17a it is seen that hot gas (red color) from the inlet cavity flows onto the outlet part of the shroud in Var.6. Figure 17b shows how the injection of cool air with mass flow rate of G_{cool}/G_{gas} = 1% through the profiled slot on the shroud surface isolates the shroud surface downstream of the fin from the hot gas passing through the tip clearance in Var.10.

Figure 17c shows the flow pattern downstream of the fin but with the distribution of total temperature T_w^* over an expanded temperature range in order to point out the cool area on the shroud surface more clearly.

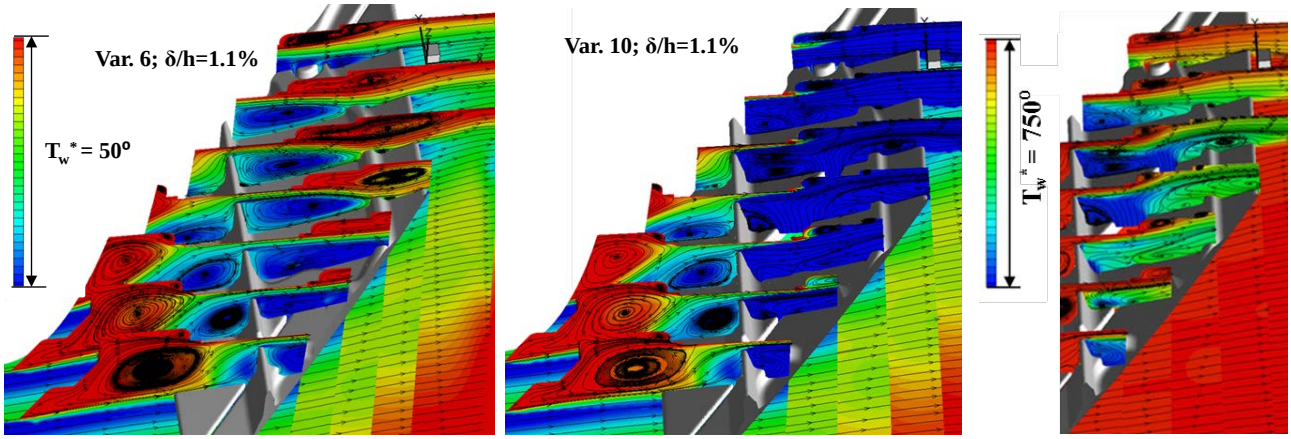

a) b) c)

Figure 17: Temperature distribution at the tip area in Var.10
a - streamlines and total temperature distributions in sections along shroud for Var.6
b - streamlines and total temperature distributions in sections along shroud for Var.10
c - total temperature distribution T_w^* for Var.10 over the expanded temperature range

CONCLUSIONS

1. The obtained numerical results concerning the flow structure around the shroud and stage efficiency depending on the shroud shape and tip clearance values have been validated by means of comparison between the test data obtained on an experimental stage with the shrouded blade and numerical data obtained for the experimental stage. The good correspondence between the test and numerical data confirmed reliability and credibility of the numerical approach.
2. The numerical approach has enabled the detailed investigation of flow structure within the tip clearance around the shrouds of various shapes. As a result, it has been confirmed that change of tip clearance leakage and losses in shrouded blades correlate with the change of vortex form, size and intensity along the shroud in the circumferential direction.
3. The unshrouded blade was the most efficient among the geometries investigated at the small relative tip clearances. The stage with unshrouded blade has a benefit in efficiency over the stage with partially shrouded blade at $\delta/h < 1.35$. At the same time the stage with unshrouded blade has a benefit in efficiency over the stage with fully shrouded blade for $\delta/h < 0.53$. These results can serve

as a justification for use of unshrouded blades on the condition that a reasonable minimum tip clearance is secured by a special control system.
4. Complicated casing design with many cavities results in an unfavorable flow structure and vortex system in the blade tip area, contributing to generation of various losses. Reduction of number of cavities as well as the free space in the area in general leads to diminished vortex intensity and losses; however, removing the vortices altogether nullifies the associated sealing features, which has negative implications on the efficiency.
5. In order to minimize the risk of shroud overheating, two variants of shroud cooling have been considered. The more efficient of the two was the injection of cool air through a profiled slot downstream of the fin. In this case the cooling air isolates the outer shroud surface from the hot gas passing through the tip clearance.

ACKNOWLEDGEMENTS

The authors gratefully acknowledge Igor Manaev for conducting the FLUENT calculations, Anatoly Shunnin for preparation of the computing models.

REFERENCE

Denton J. D., (1993), Loss Mechanisms in Turbomachines, ASME - Paper 93-GT-435.

Harvey, N. (2004), Aerothermal Implications of Shroudless and Shrouded Blades. Turbine Blade Tip Design and Tip Clearance Treatment. VKI Lecture Series LS 2004-02.

Wallis, A. M., Denton, J. D., Demargne, A. A. J., (2000) , The Control of Shroud Leakage Flows to Reduce Aerodynamic Losses in a Low Aspect Ratio, Shrouded Axial Flow Turbine, ASME-Paper 2000-GT-475

Pfau A., Kalfas A.I., Abhari R.S**.,** (2004), Making Use of Labyrinth Interaction Flow, ASME - Paper GT2004-53797

Porreca L., Behr T., Schlienger J., Kalfas A.I., Abhari R.S., Ehrhard J., Janke E.,(2005), "Fluid Dynamics and Performance of Partially and Fully Shrouded Axial Turbines" ASME Journal of Turbomachinery Oct, Vol. 127.

Nirmalan, N. V., Bailey, J. C., (2005), "Experimental Investigation of Aerodynamic Losses of Different Shapes of a Shrouded Blade Tip Section". ASME GT2005- 68903.

Gier, J., Engel, K., Stubert, B., Wittmaack, R.,(2006) Modeling and Analysis of Main Flow – Shroud Leakage Flow Intection in LP Turbines, ASME Paper GT2006-9073

Adami P., Milli A., Martelli F., Cecchi S., Comparison of Different Shroud Configurations in High-Pressure Turbines Using Unsteady CFD, 2006, ASME Paper GT2006-90442

Porreca, L., Kalfas1**,** A. I., Abhari, R.S., (2007), Optimized Shroud Design for Axial Turbine Aerodynamic Performance, ASME Paper GT2007- 27915

Rosic, B., Denton J. D., Curtis, M. E., (2007), The Influence of Shroud and Cavity Geometry on Turbine Performance – An Experimental and Computational Study, Part I: Shroud Geometry. ASME Paper GT2007- 27769

Barmpalias, K. G., Abhari, R. S., Kalfas, A. I., Shibukawa, N., Sasaki, T.,(2012) "The Impact of Rotor Inlet Cavity Volume and Length Scale on Efficiency." ASME Paper GT2012 - 68076.

Yoon, S., Curtis, E., Denton, J., Longley, J.,(2014) "The effect of clearance on shrouded and unshrouded turbines at two levels of reaction", Journal of Turbomachinery, 136:021013-1, 2014

Guyader S.L., Démolis J., Munoz J., (2016), Effect of Tip Shroud Geometries on Low Pressure Turbine Performance, ASME Paper GT2016- 56006

Granovskiy, A., Afanasiev, I., (2018), "Effect of Tip Shroud Geometries on Last Stage Efficiency" ASME GT2018-75416, pp.8.